

**Projecting Global Changes in Land Use and Ecosystem  
Services Using SEALS (Spatial Economic Allocation Landscape  
Simulator)**

Authors: Justin A. Johnson<sup>1,2,\*</sup>, Sumil K. Thakrar<sup>2,3</sup>

<sup>1</sup>Department of Applied Economics, University of Minnesota, St Paul,  
MN, USA

<sup>2</sup>The Natural Capital Project, University of Minnesota, St Paul, MN,  
USA

<sup>3</sup>School of GeoSciences, University of Edinburgh, Edinburgh, Scotland,  
UK

\*Corresponding Author: jajohns@umn.edu

This manuscript is currently a non-peer reviewed preprint submitted to  
EarthArXiv. As such, this manuscript has not yet been formally  
accepted in a peer-reviewed journal. Subsequent versions of this  
manuscript may have slightly different content.

# Projecting Global Changes in Land Use and Ecosystem Services Using SEALS (Spatial Economic Allocation Landscape Simulator)

Justin A. Johnson<sup>1,2,\*</sup>, Sumil K. Thakrar<sup>2,3</sup>

<sup>1</sup>Department of Applied Economics, University of Minnesota, St Paul, MN, USA

<sup>2</sup>The Natural Capital Project, University of Minnesota, St Paul, MN, USA

<sup>3</sup>School of GeoSciences, University of Edinburgh, Edinburgh, Scotland, UK

\*Corresponding Author: jajohns@umn.edu

December 17, 2024

## Abstract

Understanding how economic systems and ecosystems interact across space is crucial to ensure societal needs are met without compromising environmental quality. Spatially explicit economic models usually describe human activities and ensuing land-use dynamics at a resolution that is too coarse (typically 10–1000 regions) to understand how these affect many biophysical processes, including ecosystem service supply (which requires billions of 300m or finer grid-cells). Several land-use change models exist that allocate coarse land-use changes at finer spatial scales, but there is no general, global, computationally tractable tool for downscaling to the spatial scale appropriate for understanding landscape and ecosystem change across different land-system scenarios. Here, we present a new model, the Spatial Economic Allocation Landscape Simulator (SEALS), which generates global, high resolution land-use, land-cover maps from coarse projections of land-use change. SEALS advances land-use change modeling research in several ways: it uses a novel machine-learning algorithm to empirically calibrate its parameters; it is a generalized approach that can be applied to very different types of projections within earth-economy models; and it is computationally efficient, generating global results at 300m resolution in approximately 1 hour on a laptop computer. We develop SEALS, and apply it to downscale 6 global scenarios of land-use change from the Shared Socioeconomic Pathways (SSPs) to 300m resolution, which we make publicly available, allowing researchers to project global, fine-scale changes in ecosystem services. For carbon storage and sequestration, we find that, from 2021 to 2100, the SSPs considered result in reductions in carbon storage and sequestration by 3–21%, and baseline results are 9.17% lower than conventional estimates using low-resolution inputs. Consistent with prior estimates, we find that SSPs 3 and 4, which lead to large amounts of tropical deforestation, result in the largest carbon losses, further exacerbating the climate impacts.

# 1 Introduction

Economic activity is a major driver of global changes in land-use and land-cover (hereafter, simply “land-use”), including deforestation, agricultural production, and environmental pollution [1]. Understanding where those environmental changes happen at fine spatial scales—typically 30- to 300m grid-cells [2]—is key to understanding their full environmental effects [3] [4]. Emerging research creates linked earth-economy models [5] [6] [7] that compute how the economy impacts nature, and vice versa, to assess the performance of different sustainability policies. However, application of such models is challenging because it requires assessing human behavior at many different spatial scales while describing very different types of phenomena, such as international trade or reliance on ecosystem services.

High resolution land-use maps derived from satellite data, such as those from the European Space Agency’s Climate Change Initiative (ESA-CCI) [8], can be used to estimate current or historic provision of ecosystem services [9]. However, present-day land-use maps do not let us analyze counterfactuals, policy scenarios or future projections. Although models increasingly link economic activities to changes across space, most notably the integrated assessment models (IAMs) used to define the Shared Socioeconomic Pathways (SSP) scenarios [10] and their representation of land-use change [11], they typically only do so at spatial resolutions that are too coarse to understand many biophysical processes and the provision of ecosystem services [12].

Several land-use change downscaling models have been developed that can estimate high resolution land-use changes from coarser estimates such as those from IAMs. Such downscaling models use high resolution spatial correlates and equations that govern the conversion between different types of land. However, there is no general, global, empirically-calibrated tool for downscaling land use changes to this scale that is computationally tractable. The closest peer-reviewed option for this type of downscaling is CLUMondo [13] [14], but this model is limited to  $4,000 \times 4,000$  pixels, which is significantly less than the  $129,600 \times 64,800$  pixels in LULC maps from ESA-CCI. Another option, the land-use change downscaling algorithm within the GLOBIO 4 model [15], is able to produce global LULC maps at the desired resolution, but it uses heuristic suitability relationships that are not calibrated against observed changes. Other approaches in the literature provide methods for downscaling LULC data based on multinomial logistic regression (e.g., [16]) or more recent extensions using generalized additive model identified for each land-use class [17]. The approach in Hoskins *et al.* [17] provides 1km resolution results, though prior to downscaling, it aggregates Land Use Harmonization (LUH2) data into 61 bioregions. This means that the amount of land-

use change in coarse grid-cells in the LUH2 data do not necessarily match the total of the downscaled result.

In this paper, we present the first global, high resolution, empirically-calibrated downscaling model, the Spatial Economic Allocation Landscape Simulator (SEALS). SEALS is an open-source land-use change prediction model that is very general in its construction, allowing the user to easily incorporate, for example, their own sets of spatial correlates. For users without their own data, SEALS provides a high-quality, curated set of the best global, publicly available base-data for land-use change prediction. SEALS can predict global changes in land-use at the 300m level, and can do so on a laptop computer within approximately 1 hour. Furthermore, it is empirically calibrated on observed historical changes in land-use, so that it can downscale potential land-use changes in line with past observations.

Simplified versions of the SEALS methodology have recently been used to generate specific scenarios for a single land-use type, maize expansion [18], and for particular conservation policy goals [5] [19]. Here, we advance the SEALS methodology and present a full, general, and flexible land-use change model that can downscale changes in all land-use types simultaneously, and can be used for any land-use change or projection, with empirically calibrated parameters. We train SEALS parameters on observed time-series data on land-use changes from 2000–2015.

We use the model to downscale global changes in land use for each RCP-SSP scenario to 300m resolution. By contrast, a recent, notable study [20] only estimated changes in land use for RCP-SSP scenarios at  $0.05^\circ$  ( $\sim 5\text{km}$ ) resolution, which is inadequate for estimating changes in many ecosystem services. By downscaling to such a high spatial resolution worldwide, we are able to estimate the changes in carbon sequestration associated with global changes in projected land use. Previous studies have only estimated these changes for regions such as the United States ([21], the United Kingdom [22], or Europe [23], or have estimated global changes in carbon sequestration based on coarse land use projections [24] that are inadequate because changes in carbon sequestration depend on where land-use change happens at small spatial scales. Only by examining high resolution, land-use driven changes in ecosystem services can we properly account for the full range of benefits and costs of our socio-economic and climate projections.

## 2 Methods

Here, we advance the development of the SEALS model, previously described in [5], [18]; and [19]. SEALS identifies how a coarse projection of land-use change can be downscaled to higher resolutions in a way that best matches historical patterns of change. SEALS does so by estimating the probability of land-use transitions, which is modeled using 3 components: land constraints, land suitability, and adjacency effects (see 2.1, 2.2, 2.3; Supplementary Information 7.1), 7.2, 7.3. SEALS uses the overall probability of land use transitions to estimate, for any proposed coarse projection of land-use change, where that land-use change is most likely to occur (see 2.4; Supplementary Information 7.5). Although SEALS is a very general and flexible model, we describe an implementation of the model that is useful for estimating ecosystem services in Section 2.5 (also see Supplementary Information 7.9). For any particular implementation of SEALS, the parameters can be calibrated against historical land-use data (see 2.6; Supplementary Information 7.6). Finally, we describe how we estimate changes in carbon storage and sequestration in Section 2.7.

### 2.1 Land constraints

Land constraints describe the eligibility for any region to transition from its initial land-use class to any other land-use class (e.g., the middle of a lake is not eligible to transition into a city). Land constraints not hard-coded into the model and are specified by the user as input parameters to the model. For example, it is possible to relax land constraints by allowing water to transition to urban land. It is also possible to specify weights (values between 0 and 1) rather than constraints. Unlike other model parameters, land constraints are not empirically calibrated.

### 2.2 Land suitability

Land suitability describes how the probability of any region to transition to any land-use class depends on colocated spatial input variables. Input variables may include the initial land-use classification, meteorological and soil variables, or results from land-use specific models, such as process-based crop models, along with any other variables that the user specifies (which may or may not contribute to the land suitability, and may or may not be correlated with each other). In general, SEALS allows for the relationship between the spatial variables and the probability of land-use transitions to vary across space. For example, we want to capture

the fact that forest land may be more likely to transition to cropland in South America than in Africa, even if all other specified variables are constant across the regions.

### 2.3 Adjacency effects

Adjacency effects refer to how the probability of any region to transition to any land-use class depends on the land-use classes of surrounding areas. In general, land-use types are not randomly distributed in space but are rather subject to strong spatial patterns related to the fact that neighboring land-use types affect the probability of each other’s transition. For example, an agricultural field in a rural area surrounded by other agricultural fields is unlikely to become urban land, whereas an agricultural field near a city is likely to become urban land (see Fig. S1). These “adjacency effects” are empirically estimated in SEALS using layered spatial convolutions that can model any distance relationship (see Supplementary Information 7; Fig. S1), which is a novel and flexible approach for handling adjacency.

### 2.4 Allocating changes in land use

After estimating the probability of each region to transition to each land-use class, SEALS allocates (coarse) projected changes in land use to these regions sequentially in rank order (i.e., from most probable to least probable), until there is no more area to convert. In general, the result can depend on which land-use type is allocated first. Following Johnson *et al.* [25], SEALS allocates very small amounts, repeating until all the land is allocated. The choice of amount of land to allocate at each step can be made to decrease as the amount of projected land remaining in each land-use type decreases. For small enough amounts of land, the ordering of the land-use types makes very little difference to the result [25].

### 2.5 Implementation

We implement the model for use in spatially downscaling coarse, global land-use change predictions given by [11], for the following choices of Representative Concentration Pathways (RCP) and Shared Socioeconomic Pathways (SSP) (hereafter, referred to as “RCP-SSP scenarios”): RCP 2.6, SSP 1; RCP 3.4, SSP 4; RCP 4.5, SSP 2; RCP 6.0, SSP 4; RCP 7.0, SSP 3; and RCP 8.5, SSP 5. The RCP-SSP scenarios are standardized pathways exploring how socioeconomic, environmental, and technological change might occur in the coming decades; a more complete description of the RCP-SSP scenarios is given by [11].

The outputs generated by this implementation are those needed for models that analyze the environmental impacts of land-use changes on ecosystem services, such as with the InVEST (Integrated Valuation of Ecosystem Services and Tradeoffs) suite of ecosystem service models [26].

In this implementation, there are 7 discrete land-use classes, corresponding to land-use classes given by the European Space Agency Climate Change Initiative (ESA-CCI). These are: urban, cropland, grassland, forest, non-forest natural, water, and barren land. There are 1.036 million source regions  $i$ , corresponding to each  $0.25^\circ$  ( $\sim 30\text{km}$ ) grid-cell in the coarse, global land use predictions for each RCP-SSP scenario. A unique set of parameters is identified for each region corresponding to each  $1.0^\circ$  ( $\sim 110\text{km}$  grid-cell) tile on earth using the calibration algorithm described above.

For calibration, the initial land-use map is the ESA land-use map from years 2000 until 2015. Once the set of optimized parameters are found, the projections from RCP-SSP scenarios, calculated as changes from 2015, are applied to the 2015 ESA land-use map for the years 2021, 2030, 2050, 2070 and 2100. Other than the land-use maps, the spatial predictors in the model are: sand content (%), silt content (%), soil bulk density, soil cation exchange capacity, soil organic content, strict protected area, air temperature ( $^\circ\text{C}$ ), travel time to market (min), presence of wetlands, altitude (meters), above ground carbon ( $\text{Mg ha}^{-1}$ ), clay content (%), soil pH, population, and precipitation (mm) (see Table S1 for all data sources and citations).

The adjacency effects have the potential to vary differently at different spatial scales. In this implementation, we chose to focus on two scales (See Supplementary Information for more details). We trained the coefficients defined in Table 1 uniquely for each  $1^\circ$  tile on Earth, removing any tile where there was no projected change in the LUH2 data (which drops, for instance, oceanic tiles). The total number of solved parameters is large: 43 input layers multiplied by 5 changing land-use classes identified for 17,368 valid tiles generates 3.73 million total coefficients to estimate. These trained parameters are publicly available in the provided data repository, and can be used in other projects.

## 2.6 Parameter estimation

The SEALS model has several parameters whose values are to be determined empirically (see Supplementary Information 7 for more details). Although sensible parameters may be chosen based on expert opinion [18], the SEALS model allows for more empirically guided and quantitative approaches to parameter estimation, that are easier to validate and easily

allow for the parameters to vary spatially. For this implementation of SEALS, a machine learning approach is used to estimate the parameters, where a step-wise search algorithm chooses parameters until a loss function is locally minimized. We employ a loss function that represents the normalized absolute difference between Gaussian convolutions of the predicted land use (based on some choice of parameters) and the empirically observed land use (see Supplementary Information 7 for more details).

## 2.7 Ecosystem service estimation

To show how SEALS can be used to estimate global ecosystem service provision, we run the Carbon Storage and Sequestration model from InVEST [26] to calculate global carbon storage estimates for each year and RCP-SSP scenario, using the Intergovernmental Panel on Climate Change (IPCC) tier-1 carbon sequestration calculation method [27].

## 3 Results

The global SEALS simulations described in Section 2.5 for estimating land-use changes at 300m resolution required 62 minutes (system: 10<sup>th</sup> generation Intel i7 processor). Unlike other land-use change models, SEALS is fully parallelized and is not limited by available computer memory, allowing for fast, tractable computation of high resolution, global land-use maps.

We use SEALS to estimate high resolution (300m) changes in land-use for each RCP-SSP scenario for years 2021, 2030, 2050, 2070 and 2100 (see Figure 1 for global maps, and Figure 2 for a sample illustration). A dataset of our results is publicly available (see 5), providing the first comprehensive set of land-use change estimates based on the RCP-SSP scenarios that are of suitable resolution to be used in ecosystem service models such as InVEST.

Figure 3 shows that, in all RCP-SSP scenarios considered here, global above-ground carbon storage is reduced in 2100 relative to 2021. This is especially true for scenarios in which there is a large amount of deforestation, such as RCP 3.4 SSP 4.

We also compared our carbon storage results to a method that calculates carbon storage based only on the coarse input data on land-use change. For the coarse resolution estimate, we first calculated a coarse map of carbon storage by upscaling our carbon estimate from the baseline year (2015), thereby washing-out the fine-grain detail of our improved LULC map (See Figure 4 for illustration). Next, we calculated carbon loss by following a method

commonly used in coarse-scale carbon accounting approaches (*e.g.*, [28]), in which we assume that every hectare of agricultural expansion lowers carbon storage by the ratio of carbon present in forest LULC classes divided by the carbon present in agricultural LULC classes (specifically, 92.7%, based on the values in this region using the IPCC method). We found that total carbon storage in the region would be 59.5 Mt, which would be an overestimate by 9.17%. Although these carbon calculations are highly simplified, the large range of estimates shows that using high resolution estimates are very important for calculating one important ecosystem service. Future research could be done to compare our results to carbon sequestration results from a dynamic global vegetation model [29], or to show more fully the degree to which different ecosystem services are affected by high resolution heterogeneity.

## 4 Discussion

In this paper, we described the SEALS model, a new, computationally tractable, global, open source, replicable, and empirically calibrated land-use change model. SEALS is a general and flexible model, allowing the user to specify, for example, which land-use classification system to use (including whether it is discrete or continuous); the number and type of spatial predictors to use to determine the suitability of land to transition; the output spatial resolution; and the spatial scales of adjacency effects. Further, the parameters used in describing the relationships between the input variables and the probability of land transitions are not hard-coded into SEALS; rather, they can either be either specified by the user or empirically calibrated, depending on the user's needs.

As well as presenting a new model, here we use the model to derive the first set of land-use change estimates based on the RCP-SSP scenarios that are of suitable resolution to be used in ecosystem service models. Obtaining high resolution land-use results such as these are critical for understanding interactions between people and nature, which is evidenced by multiple publications that would not have been possible without such downscaling techniques (*e.g.*, [3] [5] [9] [18]). The results from these studies depended greatly on the exact location where land-use change was projected.

Our estimates of high resolution land-use change from the RCP-SSP scenarios rely on directly downscaling coarse (15-arcminute, or  $\sim 30\text{km}$ ), gridded land-use change estimates [11] derived from multiple IAMs. Because many of the underlying IAMs are computed on a much smaller number of regions (*e.g.*, 26 regions for IMAGE), there were unavoidable artefacts across coarse grid cells, where changes tend to cluster on the border of each source region. This happens when the projected change has not been observed in the historical data, and might

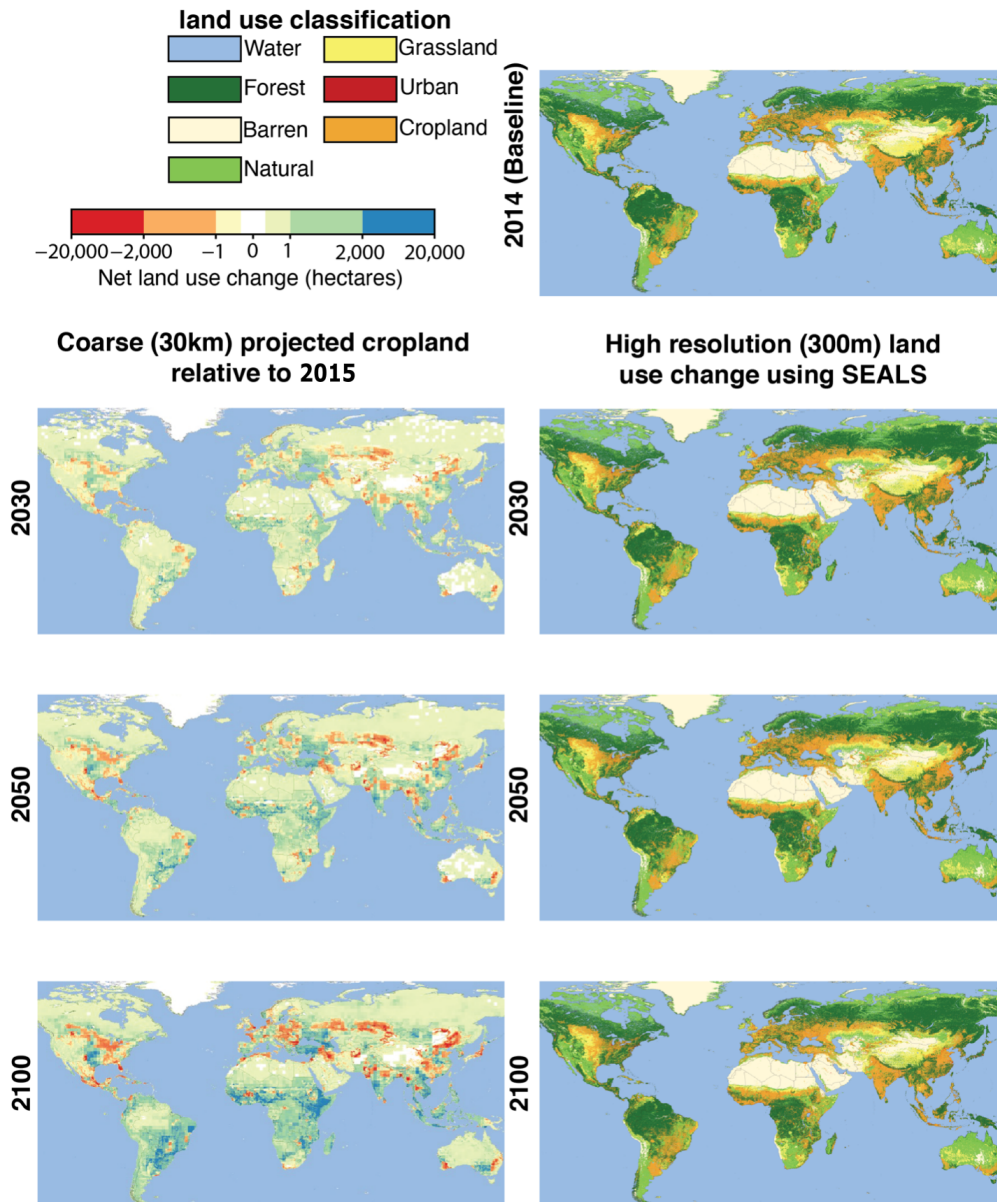


Figure 1: High resolution changes in land-use from 2030–2100 relative to the 2015 baseline (*top right*) as predicted by SEALS (*right column*) from input coarse projections of each land-use type (*left column* shows input coarse projections of cropland as an illustration).

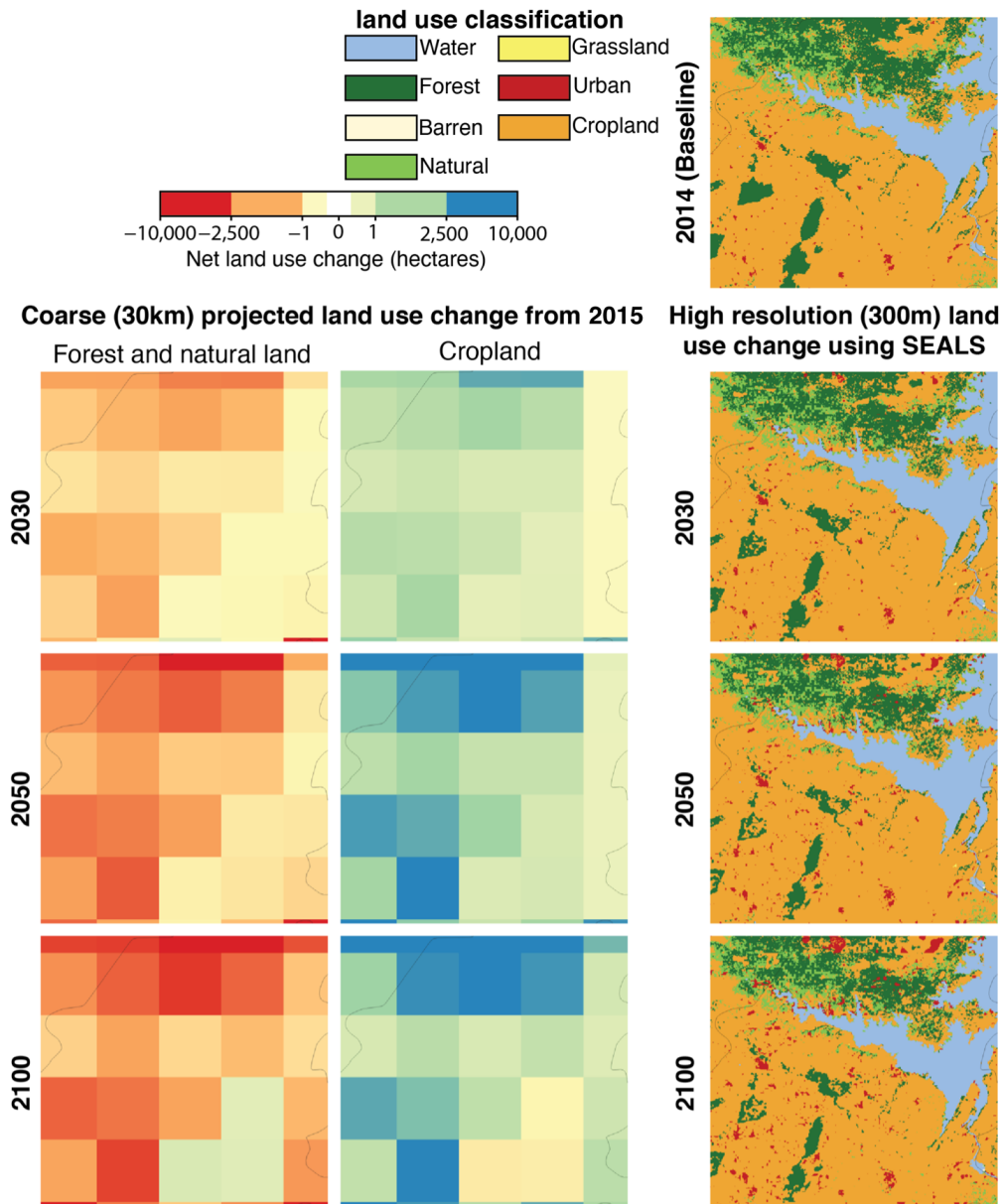


Figure 2: High resolution changes in land-use from 2030–2100 for RCP8.5 SSP5 relative to the 2015 baseline (*top right*) for a sample region, as predicted by SEALS (*rightmost column*) from input coarse projections of each land-use type (*leftmost column* and *middle column* show input coarse projections of forest/natural land and cropland as an illustration).

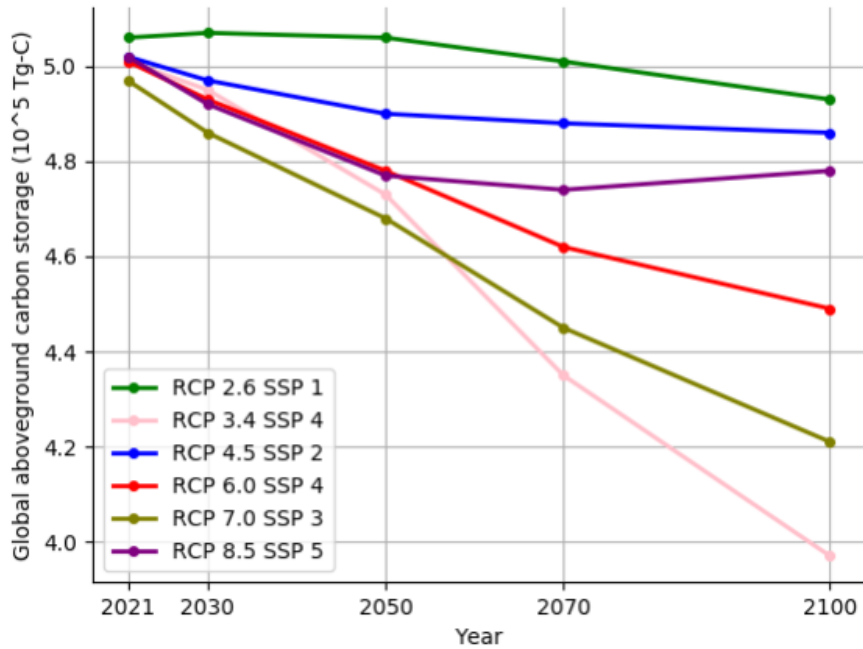


Figure 3: Global, above-ground carbon storage by each RCP-SSP scenario for 2021–2100.

represent an extremely large or improbable change. Where the training data contains enough observed changes, the artefacts are largely removed. Our approach, that runs SEALS directly on the coarse, gridded land-use change estimates, maintains consistency across the different IAMs and has increased spatial realism. Future work may combine the coarse downscaling approach described in [11] with the fine-scale downscaling approach using SEALS, to alleviate some of the issues.

SEALS can be run with a wide variety of inputs, including either the coarse-gridded or regional-polygon representations of land-use change in the IAMs. This flexibility has been critical in recent applications of SEALS in earth-economy modeling [5] [6], which downscaled land-use change predicted by the GTAP-AEZ model [28] [30] based on 341 regions and agro-ecological zones (rather than coarse-gridded projections). By maintaining input flexibility, SEALS is able to downscale land-use change across the wide range of methods used within global sustainability models. For example, future work will link SEALS into the MAgPIE IAM model [31].

SEALS currently only provides the projected land-use change as output, but it could be augmented to provide the standard error, uncertainty bounds, or a distribution of potential land use changes. Additionally, as discussed above, SEALS currently takes its coarse land use

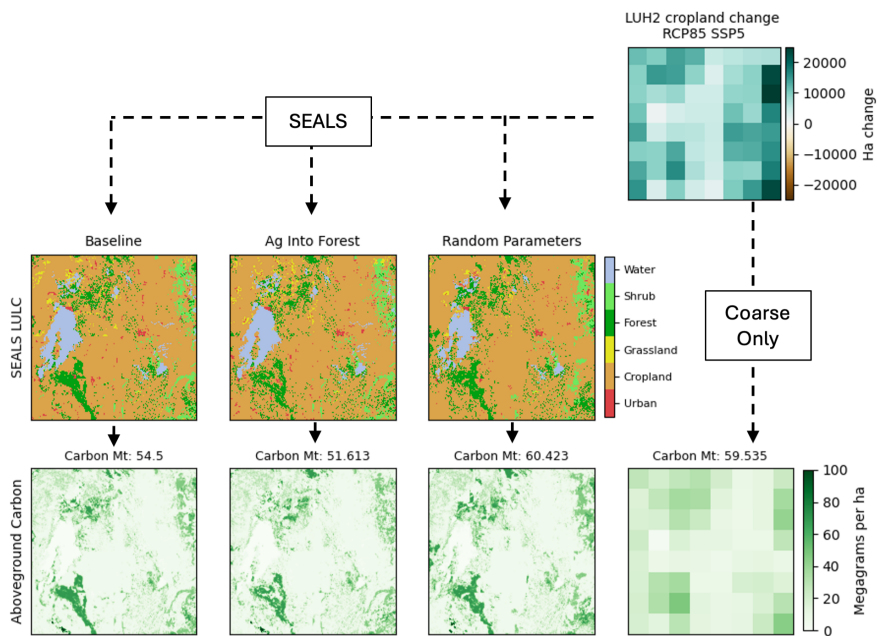


Figure 4: Estimated changes in above-ground carbon in 2050 (*bottom row*) under scenario RCP8.5 SSP5, using different assumptions for downscaling the coarse changes (*top right*) to a finer spatial scale (*middle row*) using SEALS. The “Baseline” SEALS result uses empirically calibrated parameters derived from past changes in land-use; “Ag Into Forest” uses parameters that preferentially convert forest into agriculture, as is commonly assumed in land-use models; “Random Parameters” uses a randomly assigned set of SEALS parameters. We also estimate above-ground carbon without downscaling (*bottom right*).

change inputs as given, but, in practice, they are likely to have errors. Further research could modify SEALS to assume that the coarse land use inputs are observed with some error (such as by using a Bayesian hierarchical framework), allowing the algorithm to modify the coarse projections to result in fewer artefacts. A further area for improvement is to greatly extend the range of convolutional relationships considered. Specifically, methods within machine learning that utilize convolutional neural networks are performing computationally similar tasks (though they are applied to a very different domain). Advances from this field, or related methods that use generative adversarial networks to simulate satellite photography, could be used to further expand the predictive power of SEALS.

SEALS has many potential uses. Its ability to cross spatial resolutions from (typically coarse) economic land use projections to (typically fine-scale) requirements for environmental models is one major application. Here, we provide the first empirically-calibrated land use change estimates suitable for calculating ecosystem service models globally. We provide a database of the projections for 6 RCP-SSP scenarios out to 2100, ready for use in models such as InVEST to estimate changes in ecosystem services that will result from each scenario. Many other models, such as those described in a recent ecosystem service intercomparison project [3], were limited by the need to have high resolution land-use inputs. This includes air quality models such as such as InMAP, which has grid cells as small as 4 km globally [32]. Because air quality health impacts are felt strongly at a local scale, understanding how land-use change impacts air quality worldwide may benefit from using SEALS [33]. For these applications, global land use projections from integrated assessment models estimated at 30km resolution or coarser may have large inaccuracies. Overall, to understand interconnections between people and nature that exhibit complex spatial heterogeneity, it is necessary to increase the resolution of our models.

## 5 Data Access & Code Availability

All data inputs and outputs, along with all code used, is open-source and readily available. Data may be accessed at <https://doi.org/10.5281/zenodo.14506512>.

Code is available at <https://github.com/jandrewjohnson/seals>.

## 6 Acknowledgements

We thank Patrick José von Jeetze for comments.

## References

- [1] Eduardo Sonnewend Brondízio, Josef Settele, Sandra Diaz, and Hien Thu Ngo. Global assessment report on biodiversity and ecosystem services of the intergovernmental science-policy platform on biodiversity and ecosystem services. 2019.
- [2] Kenneth J Bagstad, Erika Cohen, Zachary H Ancona, Steven G McNulty, and Ge Sun. The sensitivity of ecosystem service models to choices of input data and spatial resolution. *Applied Geography*, 93:25–36, 2018.
- [3] HyeJin Kim, Isabel MD Rosa, Rob Alkemade, Paul Leadley, George Hurtt, Alexander Popp, Detlef P Van Vuuren, Peter Anthoni, Almut Arneth, Daniele Baisero, et al. A protocol for an intercomparison of biodiversity and ecosystem services models using harmonized land-use and climate scenarios. *Geoscientific Model Development*, 11(11):4537–4562, 2018.
- [4] Melissa S Bukovsky, Jing Gao, Linda O Mearns, and Brian C O’Neill. Ssp-based land-use change scenarios: A critical uncertainty in future regional climate change projections. *Earth’s Future*, 9(3):e2020EF001782, 2021.
- [5] Justin Andrew Johnson, Giovanni Ruta, Uris Baldos, Raffaello Cervigni, Shun Chonabayashi, Erwin Corong, Olga Gavryliuk, James Gerber, Thomas Hertel, Christopher Nootenboom, et al. *The Economic Case for Nature: A global Earth-economy model to assess development policy pathways*. World Bank, 2021.
- [6] Justin Andrew Johnson, Uris Lantz Baldos, Erwin Corong, Thomas Hertel, Stephen Polasky, Raffaello Cervigni, Toby Roxburgh, Giovanni Ruta, Colette Salemi, and Sumil Thakrar. Investing in nature can improve equity and economic returns. *Proceedings of the National Academy of Sciences*, 120(27):e2220401120, 2023.
- [7] Toby Roxburgh, Karen Ellis, Justin Johnson, Uris Lantz Baldos, Thomas Hertel, Chris Nootenboom, and Stephen Polasky. Global futures: Assessing the global economic impacts of environmental change to support policy-making. 2020.
- [8] Céline Lamarche, Maurizio Santoro, Sophie Bontemps, Raphaël d’Andrimont, Julien Radoux, Laura Giustarini, Carsten Brockmann, Jan Wevers, Pierre Defourny, and Olivier Arino. Compilation and validation of sar and optical data products for a complete and global map of inland/ocean water tailored to the climate modeling community. *Remote Sensing*, 9(1):36, 2017.

- [9] Rebecca Chaplin-Kramer, Richard P Sharp, Charlotte Weil, Elena M Bennett, Unai Pascual, Katie K Arkema, Kate A Brauman, Benjamin P Bryant, Anne D Guerry, Nick M Haddad, et al. Global modeling of nature’s contributions to people. *Science*, 366(6462):255–258, 2019.
- [10] Keywan Riahi, Detlef P Van Vuuren, Elmar Kriegler, Jae Edmonds, Brian C O’neill, Shinichiro Fujimori, Nico Bauer, Katherine Calvin, Rob Dellink, Oliver Fricko, et al. The shared socioeconomic pathways and their energy, land use, and greenhouse gas emissions implications: An overview. *Global environmental change*, 42:153–168, 2017.
- [11] George C Hurtt, Louise Chini, Ritvik Sahajpal, Steve Frohking, Benjamin L Boudirsky, Katherine Calvin, Jonathan C Doelman, Justin Fisk, Shinichiro Fujimori, Kees Klein Goldewijk, et al. Harmonization of global land-use change and management for the period 850–2100 (luh2) for cmip6. *Geoscientific Model Development Discussions*, 2020:1–65, 2020.
- [12] Wolfgang Britz, Peter H Verburg, and Adrian Leip. Modelling of land cover and agricultural change in europe: Combining the clue and capri-spat approaches. *Agriculture, ecosystems & environment*, 142(1-2):40–50, 2011.
- [13] Sanneke Van Asselen and Peter H Verburg. Land cover change or land-use intensification: simulating land system change with a global-scale land change model. *Global change biology*, 19(12):3648–3667, 2013.
- [14] Sarah Wolff, Elizabeth A Schrammeijer, Catharina JE Schulp, and Peter H Verburg. Meeting global land restoration and protection targets: What would the world look like in 2050? *Global Environmental Change*, 52:259–272, 2018.
- [15] Aafke M Schipper, Jelle P Hilbers, Johan R Meijer, Laura H Antão, Ana Benítez-López, Melinda MJ de Jonge, Luuk H Leemans, Eddy Scheper, Rob Alkemade, Jonathan C Doelman, et al. Projecting terrestrial biodiversity intactness with globio 4. *Global Change Biology*, 26(2):760–771, 2020.
- [16] Nicolas Dendoncker, Patrick Bogaert, and Mark Rounsevell. A statistical method to downscale aggregated land use data and scenarios. *Journal of Land Use Science*, 1(2-4):63–82, 2006.
- [17] Andrew J Hoskins, Alex Bush, James Gilmore, Tom Harwood, Lawrence N Hudson, Chris Ware, Kristen J Williams, and Simon Ferrier. Downscaling land-use data to

- provide global 30 estimates of five land-use classes. *Ecology and Evolution*, 6(9):3040–3055, 2016.
- [18] Sangwon Suh, Justin A Johnson, Lau Tambjerg, Sarah Sim, Summer Broeckx-Smith, Whitney Reyes, and Rebecca Chaplin-Kramer. Closing yield gap is crucial to avoid potential surge in global carbon emissions. *Global Environmental Change*, 63:102100, 2020.
- [19] Justin Andrew Johnson, Uris Lantz Baldos, Thomas Hertel, Chris Nootenboom, Stephen Polasky, and Toby Roxburgh. Global futures: Modelling the global economic impacts of environmental change to support policy-making. 2020.
- [20] Min Chen, Chris R Vernon, Neal T Graham, Mohamad Hejazi, Maoyi Huang, Yanyan Cheng, and Katherine Calvin. Global land use for 2015–2100 at 0.05 resolution under diverse socioeconomic and climate scenarios. *Scientific Data*, 7(1):320, 2020.
- [21] Yanyan Cheng, Maoyi Huang, David M Lawrence, Katherine Calvin, Danica L Lombardozzi, Eva Sinha, Ming Pan, and Xiaogang He. Future bioenergy expansion could alter carbon sequestration potential and exacerbate water stress in the united states. *Science Advances*, 8(18):eabm8237, 2022.
- [22] Mark Richards, Mark Pogson, Marta Dondini, Edward O Jones, Astley Hastings, Dagmar N Henner, Matthew J Tallis, Eric Casella, Robert W Matthews, Paul A Henshall, et al. High-resolution spatial modelling of greenhouse gas emissions from land-use change to energy crops in the united kingdom. *GCB Bioenergy*, 9(3):627–644, 2017.
- [23] Catharina JE Schulp, Gert-Jan Nabuurs, and Peter H Verburg. Future carbon sequestration in europe—effects of land use change. *Agriculture, Ecosystems & Environment*, 127(3-4):251–264, 2008.
- [24] Alexander Popp, Katherine Calvin, Shinichiro Fujimori, Petr Havlik, Florian Humpenöder, Elke Stehfest, Benjamin Leon Bodirsky, Jan Philipp Dietrich, Jonathan C Doelmann, Mykola Gusti, et al. Land-use futures in the shared socio-economic pathways. *Global Environmental Change*, 42:331–345, 2017.
- [25] Justin A Johnson, Christina M Kennedy, James R Oakleaf, Sharon Baruch-Mordo, Stephen Polasky, and Joseph Kiesecker. Energy matters: Mitigating the impacts of future land expansion will require managing energy and extractive footprints. *Ecological Economics*, 187:107106, 2021.

- [26] R Sharp, J Douglass, S Wolny, K Arkema, J Bernhardt, W Bierbower, N Chaumont, D Denu, D Fisher, K Glowinski, et al. Sdr: Sediment delivery ratio—invest documentation. *InVEST*, 3(2), 2020.
- [27] Holly K Gibbs and Aaron Ruesch. New ipcc tier-1 global biomass carbon map for the year 2000. Technical report, Environmental System Science Data Infrastructure for a Virtual Ecosystem . . . , 2008.
- [28] Uris Lantz Baldos and Erwin Corong. Development of gtap version 10 land use and land cover data base for years 2004, 2007, 2011 and 2014. Technical report, Center for Global Trade Analysis, Department of Agricultural Economics . . . , 2020.
- [29] Stephen Sitch, Benjamin Smith, I Colin Prentice, Almut Arneth, Alberte Bondeau, Wolfgang Cramer, Jed O Kaplan, Samuel Levis, Wolfgang Lucht, M Thonicke Sykes, et al. Evaluation of ecosystem dynamics, plant geography and terrestrial carbon cycling in the lpj dynamic global vegetation model. *Global change biology*, 9(2):161–185, 2003.
- [30] Huey-Lin Lee, Thomas W Hertel, and Steven Rose. An integrated global land use database for cge analysis of climate policy options. In *Economic analysis of land use in global climate change policy*, pages 92–108. Routledge, 2009.
- [31] Geanderson Ambrósio, Jan Philipp Dietrich, Florian Humpenöder, Isabelle Weindl, Benjamin Leon Bodirsky, Miodrag Stevanović, Kristine Karstens, Ulrich Kreidenweis, Xiaoxi Wang, Abhijeet Mishra, et al. Magpie 4—a modular open-source framework for modeling global land systems. 2019.
- [32] Sumil K Thakrar, Christopher W Tessum, Joshua S Apte, Srinidhi Balasubramanian, Dylan B Millet, Spyros N Pandis, Julian D Marshall, and Jason D Hill. Global, high-resolution, reduced-complexity air quality modeling for pm2. 5 using inmap (intervention model for air pollution). *Plos one*, 17(5):e0268714, 2022.
- [33] Sumil K Thakrar, Justin A Johnson, and Stephen Polasky. Land-use decisions have substantial air quality health effects. *Environmental Science & Technology*, 58(1):381–390, 2023.
- [34] Joshua J Lawler, David J Lewis, Erik Nelson, Andrew J Plantinga, Stephen Polasky, John C Withey, David P Helmers, Sebastián Martinuzzi, Derric Pennington, and Volker C Radeloff. Projected land-use change impacts on ecosystem services in the united states. *Proceedings of the National Academy of Sciences*, 111(20):7492–7497, 2014.

- [35] Pascal Getreuer. A survey of gaussian convolution algorithms. *Image Processing On Line*, 2013:286–310, 2013.
- [36] Tomislav Hengl, Jorge Mendes de Jesus, Gerard BM Heuvelink, Maria Ruiperez Gonzalez, Milan Kilibarda, Aleksandar Blagotić, Wei Shangguan, Marvin N Wright, Xiaoyuan Geng, Bernhard Bauer-Marschallinger, et al. Soilgrids250m: Global gridded soil information based on machine learning. *PLoS one*, 12(2):e0169748, 2017.
- [37] Roxanne Leberger, Isabel MD Rosa, Carlos A Guerra, Florian Wolf, and Henrique M Pereira. Global patterns of forest loss across iucn categories of protected areas. *Biological Conservation*, 241:108299, 2020.
- [38] Stephen E Fick and Robert J Hijmans. Worldclim 2: new 1-km spatial resolution climate surfaces for global land areas. *International journal of climatology*, 37(12):4302–4315, 2017.
- [39] D J Weiss, Andy Nelson, HS Gibson, W Temperley, Stephen Peedell, Allie Lieber, Matt Hancher, Eduardo Poyart, Simão Belchior, Nancy Fullman, et al. A global map of travel time to cities to assess inequalities in accessibility in 2015. *Nature*, 553(7688):333–336, 2018.
- [40] Thomas Gumbricht, Rosa Maria Roman-Cuesta, Louis Verchot, Martin Herold, Florian Wittmann, Ethan Householder, Nadine Herold, and Daniel Murdiyarto. An expert system model for mapping tropical wetlands and peatlands reveals south america as the largest contributor. *Global change biology*, 23(9):3581–3599, 2017.
- [41] Justin Andrew Johnson. Globally harmonized carbon storage data. 2019.
- [42] CIESIN. Documentation for gridded population of the world, version 4 (gpwv4)., 2016.

**Supplementary Information for**  
**Projecting global changes in land use and ecosystem services using SEALS**  
**(Spatial Economic Allocation Landscape Simulator)**

## 7 Mathematical description of SEALS

Our overall goal is to find  $\widehat{Y}_{ijk}$ , the land-use change allocated to “target” (*i.e.*, high resolution) regions  $i$  within “source” (*i.e.*, coarse resolution) regions  $j$ , with land-use class  $k$ , for all  $i, j, k$ , subject to the constraint that:  $\sum_i \left( \widehat{Y}_{ijk} \times w_{ij} \right) = Z_{jk}$ ,

where  $Z_{jk}$  are the areal land-use changes in the source regions and  $w_{ij}$  are the areas of each target region. This says that overall land-use change for each  $j^{th}$  source region is equal to the summation of all  $i^{th}$  changes in the source region.

The land-use classification  $k$  can be discrete (*e.g.*, a region can either be “forest” or “cropland”) or continuous (*e.g.*, a region can be 65% forest and 35% cropland). For discrete classifications, we have the constraint that:

$$\forall ij \exists k' \text{ s.t. } \widehat{Y}_{ijk} = \begin{cases} 1 & \text{for } k = k' \\ 0 & \text{otherwise} \end{cases}$$

*i.e.*,  $\widehat{Y}_{ijk}$  takes only the values 0 and 1, and each target region has exactly one land-use type  $k'$  (for which  $\widehat{Y}_{ijk'} = 1$ ). For continuous land-use classifications, this constraint simply becomes  $\sum_k \widehat{Y}_{ijk} = 1$ . Although the SEALS model allows for both discrete and continuous land-use classifications, for simplicity we describe the SEALS model here only with reference to discrete land-use classification, which will produce outputs similar to typical land-use maps such as from the ESA-CCI.

$\widehat{Y}_{ijk}$  is found by first training  $P_{ijk}$ , the overall probability of each target zone  $i$  in each source zone  $j$  to transition to each land-use class  $k$ , on a set of observed land-use changes. Once found,  $P_{ijk}$  is then used to project future fine-scale land-use change from coarse predictions.

SEALS models the overall suitability  $P_{ijk}$  for each target zone to transition to the land-use class  $k$ , based on three main components: land constraints, land suitability, and adjacency effects. Land constraints describe the eligibility for any region to transition from its initial land-use class  $k_{ij0}$  to any other land-use class (*e.g.*, the middle of a lake is not eligible to transition into a city). Land suitability depends on spatial input variables, such as the initial land-use classification, meteorological and soil variables, or results from land-use specific

models, such as process-based crop models, along with any other variables that the user specifies. Finally, we consider adjacency effects on land-use transition probabilities in a novel and flexible way. We assume land-use types are not randomly distributed in space but are rather subject to strong spatial patterns related to the fact that neighboring land-use types affect the probability of each other’s transition (*e.g.*, an agricultural field in a rural area surrounded by other agricultural fields is unlikely to become urban land, whereas an agricultural field within a city is likely to become urban land). These “adjacency effects” are empirically estimated in SEALS using layered spatial convolutions that can model any distance relationship. The following subsections describe each of these SEALS three main components.

### 7.1 Land constraints

Land constraints are modelled by an operator  $C : \langle k, k_{ij0} \rangle \rightarrow M_{ijk}$ , that creates a matrix of 1s, except for certain pairs of  $\langle k, k_{ij0} \rangle$  where it is assigned 0, and generates a new assignment for the overall probability. For example,

$$P_{ijk'} = 0 \text{ if } (k_{ij0} = \textit{water} \ \& \ k' = \textit{urban})$$

Land constraints not hard-coded into the model and are specified by the user as input parameters to the model. For example, it is possible to relax land constraints by allowing water to transition to urban land. It is also possible to specify weights (values between 0 and 1) rather than constraints. Unlike other model parameters, land constraints are not empirically calibrated (a process we describe in Section 7.6). Because  $P_{ijk}$  is not strictly a probability, there is no need to renormalize it each time  $C$  is applied.

### 7.2 Land suitability

We want to find the contribution of land suitability to  $P_{ijk}$ , the overall suitability for land in target region  $i$  in source region  $j$  to transition to land-use  $k$ . We define a vector (with a preferred basis) of spatial variables,  $V^n$ , each element of which may or may not contribute to the land suitability. For simplicity, the variables  $i$  and  $j$  are omitted, but each element of  $V^n$  in general varies across source and target regions.

SEALS models the contribution of each of the spatial variables in  $V^n$  using a vector of parameters,  $\hat{\beta}^n \in (-\infty, +\infty)$ , such that the contribution of land suitability to  $P_{ijk}$  is

$$\widehat{\beta}^{nT} \cdot V^n$$

The user can provide arbitrary spatial variables as inputs to SEALS, such as meteorological variables, soil variables, and economic variables, regardless of whether they are correlated with each other, or whether they are expected to affect the suitability for land to transition. In particular, we are concerned with the current land-use,  $L_{ijkt_0}$ , which is classically assumed to affect the probability of land-use transitions (*e.g.*, [34]). In other words, by reordering variables, we can decompose  $V^n$  into  $\begin{pmatrix} L_{ijkt_0} \\ U_{ij} \end{pmatrix}$ , and  $\widehat{\beta}^n$  into  $\begin{pmatrix} \widehat{\beta}_1 \\ \widehat{\beta}_2 \end{pmatrix}$ .

In general, SEALS allows for the relationship between the spatial variables and the probability of land-use transitions to vary across space. *e.g.*, we want to capture the fact that forest land may be more likely to transition to cropland in South America than in Africa, even if all other specified variables are constant across the regions. To this end, we define regions  $q$  (*e.g.*, continents, or agro-ecological zones) larger than the source regions  $j$  such that  $\widehat{\beta}_{ijk} = \widehat{\beta}_{i'j'k} = \widehat{\beta}_{qk}$  for all  $i, j, i', j'$  in  $q$ .

We describe the process for empirically calibrating the parameters  $\widehat{\beta}_{qk}^n$  in Section 7.6.

### 7.3 Adjacency effects

For all  $i, j$  we can assign a distance metric  $D(i, j, i', j')$  between the target zone  $i$  in source zone  $j$  and any target zone  $i'$  in any source zone  $j'$ . We choose  $D$  to be the Euclidean distance between the centroids of  $i$  in  $j$  and  $i'$  in  $j'$ .

Then, we define our discretized Gaussian function as:

$$G_{i,j}(\sigma, i', j') = \frac{1}{2\pi\sigma^2} e^{-\frac{D^2(i,j,i',j')}{2\sigma^2}}$$

For some choice of  $\sigma$  (described below). We can apply a Gaussian convolution [35] to the current land-use, *i.e.*,

$$L'_{i'j'kt_0} = G_{ij}(\sigma, i', j') * L_{ijkt_0} = \sum_{ij} G_{ij}(\sigma, i', j') L_{ijkt_0}$$

After convolving the map, by applying the Gaussian convolution, every target zone will carry some information about the adjacent land. In the unconvoluted land-use map, by contrast,

the values in each target zone tell us only what the land-use type is within that target zone.

Adjacency effects can happen at multiple spatial scales, governed by the  $\sigma$  parameter in the Gaussian distribution. SEALS allows for multiple scales of adjacency effects by allowing the user to choose a set of parameters,  $\sigma_m = \sigma_1, \sigma_2, \dots$

The adjacency effect is then given by

$$\sum_{m,l,k} \hat{\alpha}_{qlk} G_{ij}(\sigma_m, i', j') * L_{ijkt_0}$$

Here,  $\hat{\alpha}_{qlk} \in (-\infty, +\infty)$  is a set of parameters to be empirically calibrated. Like  $\hat{\beta}_{qk}$  above, these parameters can vary over regions  $q$ .

Note that the Gaussian convolution extends over source regions  $j$  which are not in general treated as boundaries. The global boundary of the domain is handled by a zero-padding boundary extension [35]. Figure S1 illustrates how the adjacency effect from cropland and urban land on cropland expansion is calculated for Minnesota, United States of America (USA).

#### 7.4 Overall suitability of land-use transitions

We combine the equations from the above components to arrive at an equation for the overall suitability of land-use transitions:

$$P_{ijk} = C(\langle k, k_{ij0} \rangle) \left( \sum_{m,l,k} \hat{\alpha}_{qlk} G_{ij}(\sigma_m, i', j') * L_{ijkt_0} + \sum_{q,k} \hat{\beta}_{qk}^{nT} \cdot V^n \right)$$

This equation includes the values of  $C$ ,  $\hat{\alpha}_{qlk}$ , and  $\hat{\beta}_{qk}^n$ , which are to be empirically calibrated, as described in Section 7.6.

#### 7.5 Allocating changes in land use

Once we know  $P_{ijk}$  for some set of parameters, we can use it to allocate changes in land-use  $Z_{jk}$  specified at the coarse scale (*e.g.*, from our economic model or other global land-use change models) to fine scale changes in our high resolution target zones  $i$ . To do this, SEALS first generates a rank ordering of all  $P_{ijk}$  in each region  $j$ , for each land-use type  $k$ . SEALS

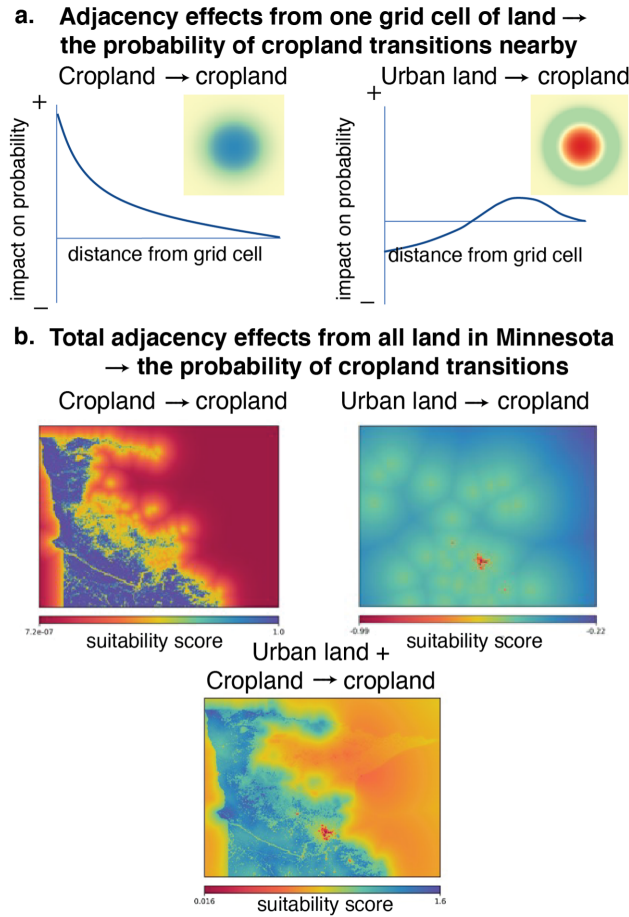


Figure S1: Explanation of adjacency effects. (a) An illustration of the adjacency effect from one grid cell of cropland (*left*) or urban land (*right*), on the probability of land-use transitions to cropland in neighboring grid cells. The images illustrate the adjacency effects in 2 dimensions, where the grid cell of crop or urban land is in the center of the circles. As the adjacency effect is isotropic, the effect can be illustrated in 1 dimension, as shown by the line graphs. (b) An illustration of the adjacency effect from current cropland (*left*) and urban land (*right*), and their sum (*bottom*), in Minnesota, USA.

then sequentially allocates the total land-use change  $Z_{jk}$  for each source region to the target regions, from most probable to least probable, until there is no more area to convert.

In general, the result can depend on which land-use type  $k$  is allocated first. Following [25], SEALS sorts the land-use types  $k = k_1, k_2, \dots$  into alphabetic order, and then allocates very small amounts  $\delta Z_{jk_1}$  of land-use type  $k_1$ , followed by very small amounts  $\delta Z_{jk_2}$  of land-use type  $k_2$  *etc.*, repeating until all the land is allocated. The choice of amount of land to allocate at each step,  $\delta Z_{jk}$ , can be made to decrease as the amount of  $Z_{jk}$  remaining in each land-use type decreases. For small enough  $\delta Z_{jk_2}$ , the alphabetical ordering of the land-use types makes very little difference to the result [25].

## 7.6 Parameter estimation

The SEALS model, as described above, is parameterized by the variables  $C$ ,  $\hat{\alpha}_{qk}$ , and  $\hat{\beta}_{qk}^n$ , whose values are to be determined. Although sensible parameters may be chosen based on expert opinion [18], the SEALS model allows for more empirically guided and quantitative approaches to parameter estimation, that are easier to validate and easily allow for the parameters to vary spatially.

Here, we describe an approach to estimate parameters in SEALS that is achieved by, (a) defining a loss function (see Section 7.7) that acts as a metric for how similar two land-use maps are, and (b) estimating the parameters using a step-wise, “greedy” search algorithm that minimizes the loss function (see Section 7.8).

## 7.7 Loss function

We first define a similarity metric  $D_G$  between two land-use maps,  $\hat{Y}_{ijk}$  and  $Y_{ijk}$ :

$$D_G(\hat{Y}_{ijk}, Y_{ijk}) = \frac{1}{2N} \sum_k \left| G_{ij}(\sigma, i', j') * \hat{Y}_{ijk} - G_{ij}(\sigma, i', j') * Y_{ijk} \right|$$

where  $G_{ij}(\sigma, i', j')$  \* represents the Gaussian convolution as described in Section 7.3, and  $N$  is the number of grid cells. The similarity metric represents the sum of the region-by-region differences between the two land-use maps, except for the fact that both land-use maps have been blurred by the convolution. This accounts for the fact that images can be similar when nearby regions have the same land-use classes, even if they do not exactly overlap.  $D_G$  ranges

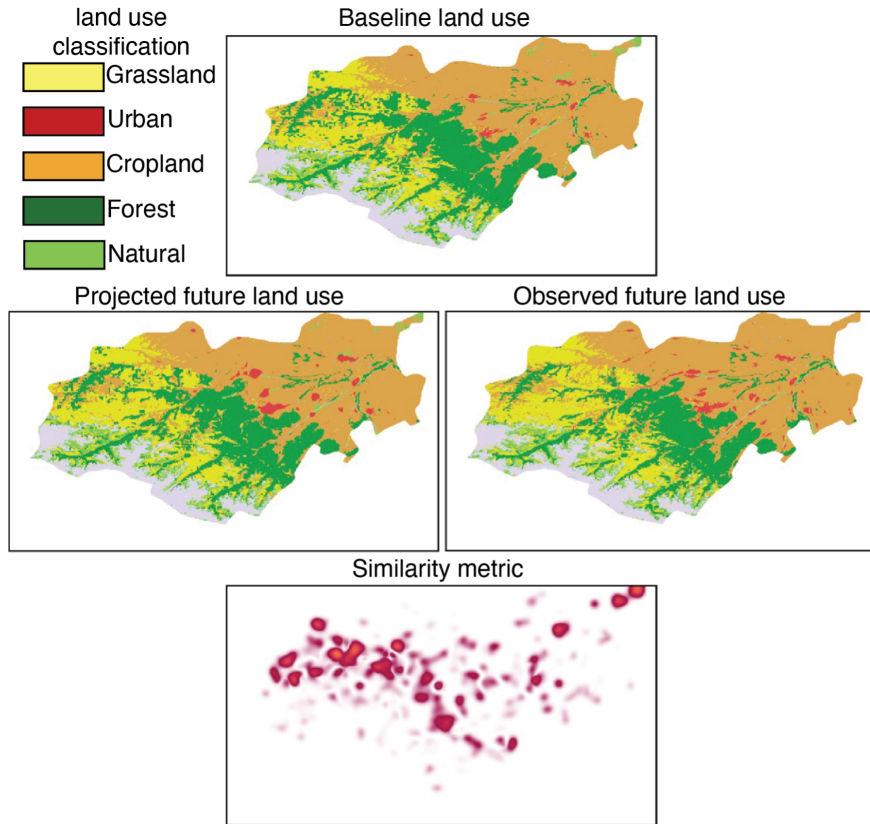


Figure S2: Explanation of the similarity metric for use in model calibration or evaluation, visualized for the Krasnodar region of Russia. The baseline land-use (*top*) and observed future land-use (*middle right*) are taken from the ESA for a sample region; the projected future land-use (*middle left*) is found using SEALS from the baseline land-use, given coarse changes in future land-use. The difference between the (convolved) projected future land-use and the (convolved) observed future land-use for all land-use types is also shown (*bottom*); the sum of these differences gives rise to the similarity metric, as can be used for model calibration or evaluation.

from 0–1: for two identical land-use maps,  $D_G = 0$ ; for two land-use maps that are exactly orthogonal (*e.g.*, one that is all forest and another that is all cropland),  $D_G = 1$ .

$D_G$  can be used to find the similarity between predicted and observed land-use maps, so as to score the predictions according to how close they match observations. For a set of land-use predictions generated by a choice of parameters,  $D_G$  can be used as a loss function, and a choice of parameters can be found that minimizes  $D_G$  and thus best predict the observed land-use change. Figures S2 and S3 illustrate how the similarity metric is found for a sample region.

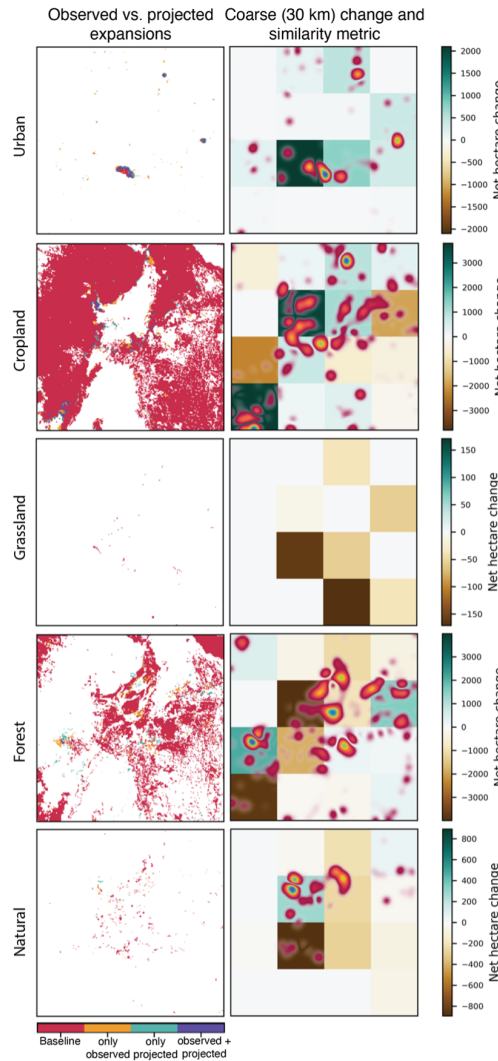


Figure S3: An illustration of comparisons between observed and projected land-use types for a region surrounding Rwanda (*left column*), alongside the input coarse land-use inputs, and the resulting similarity between projected and observed changes, for each land-use type (*right column*).

## 7.8 Calibration

To calibrate the model, we use a gradient-descent search algorithm that does the following:

- (a) sets the parameters at an initial starting value (for example, those in Table 1);
- (b) runs the SEALS model on an initial land-use map,  $L_{ijkt_0}$ , and a coarse-grained change in land-use (*i.e.*,  $Z_{jk}$ ) calculated from an observed land-use map from a later year;
- (c) uses the loss function to find how similar the predictions are to the observed land-use map, and
- (d) iteratively updates the parameters based on the value of the loss function, until no further improvements can be found.

Once we have found the correctly calibrated parameter set, we can use these parameters in the equation for  $P_{ijk}$  given in Section 7.4. Then, for any change in land-use  $Z_{jk}$ , we can arrive at our desired high resolution land-use map  $Y_{ijk}$  by again allocating the changes in land-use using the method described in Section 7.5.

## 7.9 Implementation

As we have described it, SEALS is a very general model, allowing for arbitrary spatial input variables. Here, we describe an implementation of the model for use in spatially down-scaling coarse, global land-use change predictions given by [11], for the following choices of Representative Concentration Pathways (RCP) and Shared Socioeconomic Pathways (SSP) (hereafter, referred to as “RCP-SSP scenarios”): RCP 2.6, SSP 1; RCP 3.4, SSP 4; RCP 4.5, SSP 2; RCP 6.0, SSP 4; RCP 7.0, SSP 3; and RCP 8.5, SSP 5. The RCP-SSP scenarios are standardized pathways exploring how socioeconomic, environmental, and technological change might occur in the coming decades; a more complete description of the RCP-SSP scenarios is given by [11].

The outputs generated by this implementation are those needed for models that analyze the environmental impacts of the land-use change on ecosystem services, such as with the INVEST (Integrated Valuation of Ecosystem Services and Tradeoffs) suite of ecosystem service models [26].

In this implementation, there are 7 discrete land-use classes  $k$ , corresponding to land-use classes given by the European Space Agency Climate Change Initiative (ESA-CCI). These are: urban, cropland, grassland, forest, non-forest natural, water, and barren land. There

are 1.036 million source regions  $i$ , corresponding to each  $0.25^\circ$  ( $\sim 30\text{km}$ ) grid-cell in the coarse, global land use predictions for each RCP-SSP scenario. A unique set of parameters is identified for each region  $q$ , corresponding to each  $1.0^\circ$  ( $\sim 110\text{km}$  grid-cell) tile on earth using the calibration algorithm described above.

For calibration, the initial land-use map  $L_{ijkt_0}$  is the ESA land-use map from the year 2000. Once the set of optimized parameters are found, the projections from RCP-SSP scenarios, calculated as changes from 2015, are applied to the 2015 ESA land-use map for the years 2021, 2030, 2050, 2070 and 2100. Other than the land-use maps, the spatial predictors  $U_{ij}$  in the model are: sand content (%), silt content (%), soil bulk density, soil cation exchange capacity, soil organic content, strict protected area, air temperature ( $^\circ\text{C}$ ), travel time to market (min), presence of wetlands, altitude (meters), above ground carbon ( $\text{Mg ha}^{-1}$ ), clay content (%), soil pH, population, and precipitation (mm) (see Table 1 for all data sources and citations).

The adjacency effects have the potential to vary differently at different spatial scales. In this implementation, we chose to focus on two scales, summarized by,  $\sigma_m = 1$  or 5. 1 corresponds to a short-range adjacency effect, and 5 corresponds to a long-range effect. Table 1 gives the full list of parameters used in this implementation of SEALS, and the initial values used in the empirical calibration.

We trained the coefficients defined in Table 1 uniquely for each  $1^\circ$  tile on Earth, removing any tile where there was no projected change in the LUH2 data (which drops, for instance, oceanic tiles). Data sources are noted in superscripts as follows: 1. (Lamarche *et al.*, 2017) [8]; 2. (Hengl *et al.*, 2017) [36]; 3. (Leberger *et al.*, 2020) [37]; 4. (Fick & Hijmans, 2017) [38]; 5. (Weiss *et al.*, 2018) [39]; 6. (Gumbrecht *et al.*, 2017) [40]; 7. (J. A. Johnson, 2019) [41]; 8. (CIESIN, 2016) [42].

Parameter name	Parameter Type	Urban	Crop-land	Grass-land	Forest	Non-forest natural
Urban constraint <sup>1</sup>	Constraint (C)	1	1	1	1	1
Cropland constraint <sup>1</sup>		1	0	1	1	1
Grassland constraint <sup>1</sup>		1	1	0	1	1
Forest constraint <sup>1</sup>		1	1	1	0	1
Non-forest Natural constraint <sup>1</sup>		1	1	1	1	0
Water constraint <sup>1</sup>		0	0	0	0	0
Barren & other constraint <sup>1</sup>		0	0	0	0	0
Urban suitability <sup>1</sup>	Land-use presence ( $\hat{\beta}_1$ )	0	0	0	0	0
Cropland suitability <sup>1</sup>		0	0	0	0	0
Grassland suitability <sup>1</sup>		0	0	0	0	0
Forest suitability <sup>1</sup>		0	0	0	0	0
Non-forest suitability <sup>1</sup>		0	0	0	0	0
Water suitability <sup>1</sup>		0	0	0	0	0
Barren & other suitability <sup>1</sup>		0	0	0	0	0
Sand percent <sup>2</sup>	Spatial covariates ( $\hat{\beta}_2$ )	1	1	1	1	1
Silt percent <sup>2</sup>		1	1	1	1	1
Soil bulk density <sup>2</sup>		1	1	1	1	1
Soil cation-exchange capacity <sup>2</sup>		1	1	1	1	1
Soil organic content <sup>2</sup>		1	1	1	1	1
Strict protected area <sup>3</sup>		1	1	1	1	1
Temperature <sup>4</sup>		1	1	1	1	1
Travel-time to market <sup>5</sup>		1	1	1	1	1
Wetlands presence <sup>6</sup>		1	1	1	1	1
Altitude <sup>4</sup>		1	1	1	1	1
Carbon above-ground content <sup>7</sup>		1	1	1	1	1
Clay % <sup>2</sup>		1	1	1	1	1
pH <sup>2</sup>		1	1	1	1	1
Population <sup>8</sup>		1	1	1	1	1
Precipitation <sup>2</sup>		1	1	1	1	1
Urban adjacency; near <sup>1</sup>	Adjacency variables ( $\hat{\alpha}_k$ )	10	5	1	1	1
Cropland adjacency; near <sup>1</sup>		1	10	1	1	1
Grassland adjacency; near <sup>1</sup>		1	1	10	1	1
Forest adjacency; near <sup>1</sup>		1	1	1	10	1
Non-forest natural adjacency; near <sup>1</sup>		1	1	1	1	10
Water adjacency; near <sup>1</sup>		1	1	1	1	1
Barren adjacency; near <sup>1</sup>		1	1	1	1	1
Urban adjacency; far <sup>1</sup>		2	0.4	0.2	0.2	0.2
Cropland adjacency; far <sup>1</sup>		0.2	2	0.2	0.2	0.2
Grassland adjacency; far <sup>1</sup>		0.2	0.2	2	0.2	0.2
Forest adjacency; far <sup>1</sup>		0.2	0.2	0.2	2	0.2
Non-forest natural adjacency; far <sup>1</sup>		0.2	0.2	0.2	0.2	2
Water adjacency; far <sup>1</sup>		0.2	0.2	0.2	0.2	0.2
Barren adjacency; far <sup>1</sup>		0.2	0.2	0.2	0.2	0.2

Table 1: The parameters used in this implementation of the SEALS model. The parameter type column describes how the variable is used in the SEALS model. The rightmost columns give the initial values for different land-use types. These values are updated for some parameters as the model is empirically calibrated.